A Non-Smooth-Contact-Dynamics analysis of Brunelleschi's *cupola*. An octagonal vault or a circular dome?

Valentina BEATINI

Department of Architecture and Built Environment
Northumbria University, NE1 8ST, Newcastle upon Tyne, UK
email: valentina.beatini@northumbria.ac.uk

Gianni ROYER-CARFAGNI

Department of Industrial Engineering
University of Parma, Parco Area delle Scienze 181/A, I 43100 Parma, Italy
email: gianni.royer@unipr.it
and
Construction Technologies Institute - Italian National Research Council (ITC-CNR)
Via Lombardia 49, I 20098 San Giuliano Milanese, Milano, Italy

Alessandro TASORA

Department of Industrial Engineering
University of Parma, Parco Area delle Scienze 181/A, I 43100 Parma, Italy
email: alessandro.tasora@unipr.it

Abstract

The *cupola* (dome) of Santa Maria del Fiore in Florence was ingeniously constructed by Brunelleschi using a conical bricklaying, radial-oriented toward a focus point on the central axis. Therefore, the dome is built as a surface of revolution but with parts cut away to leave the octagonal cluster vault form. This *circular* arrangement is compared with an *octagonal* horizontal corbelling in models where the dome is schematized as an assembly of rigid-blocks in frictional contact, analyzed with a Non-Smooth-Contact-Dynamics (NSCD) approach. The high indeterminacy of the contact reactions implies considerable difficulties in their determination, which are faced *via* a regularization procedure by adding a compliance at the contact points in representation of the deformability of the mortar joints. Numerical experiments, performed with a custom software, highlight the uniform flow of forces in the Brunelleschi arrangement, but evidence the disturbances induced by the herringbone spirals, mainly used for construction

purposes, which are overloaded along the meridians and very weak in the direction of the parallels. This is due to the vertical narrow disposal of the blocks, which increases the stiffness in meridional direction, but diminishes the capacity of the friction-induced forces to equilibrate the hoop stress.

Keywords: Dome, Masonry, Friction, Brunelleschi, Rigid Body Mechanics, Non-Smooth Contact Dynamics.

1 Introduction

The vaulting of the octagonal-based *cupola* of the Basilica of Santa Maria del Fiore in Florence, the masterpiece by Filippo Brunelleschi (1377-1446), started in 1420 and ended in 1436. The works for the lantern began 10 years later, following a long debate and a new competition won again by Brunelleschi, and were concluded in 1471 [26]. This is still nowadays the largest masonry dome in the world and one of the most studied and commented constructions of Christianity. It is not possible, even tentatively, to recall the main scientific works on this superb monument (a state of the art is the book by Di Pasquale [17]), but we limit to what reputed essential for our aim, which consists in the discussion, albeit on a simplified model, of the ingenues methods proposed by Brunelleschi to construct a dome without falsework following the scheme of an octagonal groin vault, which posed serious technical challenges with respect to the *cupolae* of revolution. To this aim, numerical experiments are made with a custom software implementing a Non-Smooth-Contact-Dynamics (NSCD) approach, where the high indeterminacy of the contact reactions is by-passed with a regularization procedure adding a compliance at the contact points, representative of the deformability of the mortar joints.

The Cathedral works had started in 1296 developing the original project by Arnolfo di Cambio and the base of the octagonal drum had been ready since 1314-1315 [26]. Although nobody really knew how to construct the dome, its octagonal shape must have been defined, because it is represented in a 1355 fresco by Andrea di Bonaiuto in the *Cappellone degli Spagnoli* of the Basilica of Santa Maria Novella, and since 1367 a scale model was available in one of the side aisles of the growing cathedral. Indeed, the dome appeared as a polygonal groin vault that, following the medieval technique, needed to be built on a wooden armature or falsework, also called *centering*[1]. However, taking into account that the drum was 43 m in diameter and already almost 60 m high, it was impossible in practice to provide the timberwork [26]. Moreover, since the drum was a slender structure constructed on arches, not strengthened by the buttresses typical of Gothic Architecture, any outward thrust from the dome consequent to its possible meridional cracking, needed to be small.

[1] Leon Battista Alberti confirms that "*Testudo camura atque item fornix armamentis substitutis inducatur, necesse est*" (*The Groin vault and the barrel vault have to be constructed with the support of centering*), *De Re Aedificatoria* [1], liber III, Caput XIX.

During the long discussion that proceeded the construction, Neri di Fioravanti (1300(?)-1374) had proposed to decrease the curvature of the sections of the of the dome according to the Gothic arch following the rule known in Italy as the "*quinto acuto*" (pointed fifth), which consisted in dividing the diameter in five equal parts and drawing the curvature of the arch of the dome with 4/5 of that diameter [26]. To counterbalance the outward thrust, he also proposed to encircle the dome with stone and wooden chains. Neri also planned for the dome the rare use of a double shell, a technique used in Islamic mosques and mausoleums, as the one built in 1312 in Soltaniyeh (Iran), where the interior shell was designed for structural strength, while the exterior one offered protection from climatic actions [21].

Brunelleschi had spent several years studying the monuments of ancient Rome, in particular the Pantheon, the Minerva Temple and, probably, Nero's Domus Aurea, containing a spherical dome resting on an octagonal base [26]. Building without falsework was possible for a dome of revolution, constructed by layering one ring on the other, but not for a octagonal groin vault. Moreover, as the construction progressed, the plane of the joints would have become more and more inclined with respect to the horizontal plane, so that special countermeasures should have been required to avoid sliding of the bricks on the fresh mortar. Brunelleschi conceived a double shell with a *quinto acuto* profile, as in Figure 1(a), but with major innovative ideas.

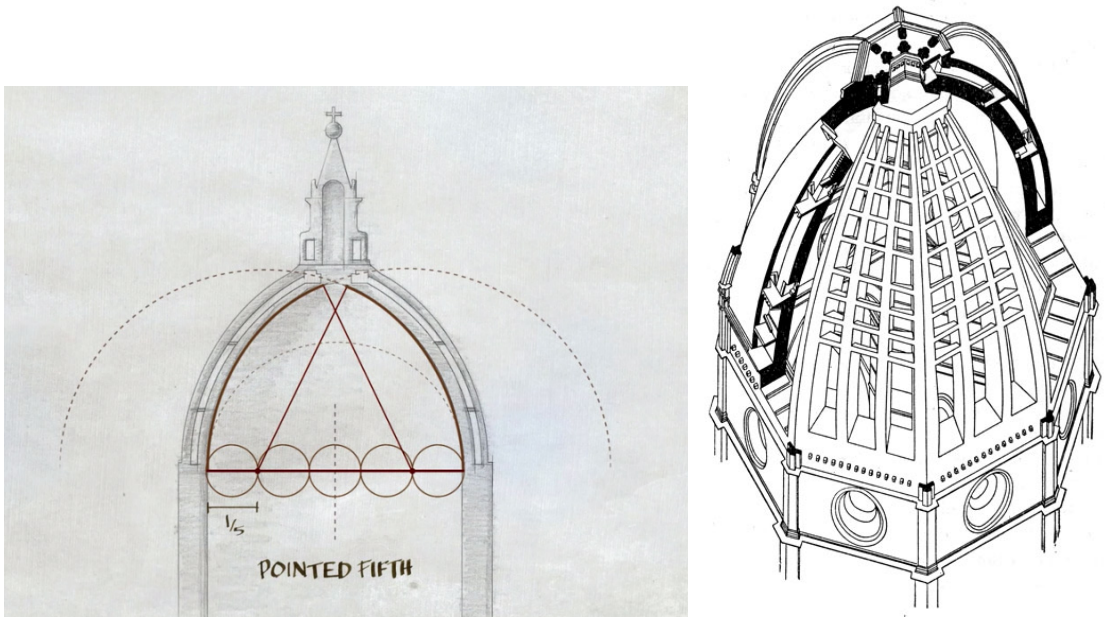

(a) (b)

Figure 1: Geometry of the dome. a) Diagram of the "*quinto acuto*", the pointed fifth arch (www.bergbuilding.com/berg-built-blog/design-build-from-concept-to-reality); b) the ribs and circles interconnecting the inner and outer vaults (from [35]).

Brunelleschi was so jealous of his work that he left no plans of the dome, and looking from the outside or the inside it is not possible to identify all the tricks of its construction, some of which are still unrevealed even after paramount studies. Although there is no universal agreement, it is commonly accepted that the disposition of the estimated 4 million bricks of various shapes followed three main criteria.

- *Internal coupling elements.* The cupola is not composed of two separated shells but it is a unique structure with internal lightening voids, because the shells are structurally coupled by 24 ribs (*sproni*), girdered by six circles (*cerchi*) of strong sandstone blocks well linked by lead-lined iron clamps [29], as schematically represented in Figure 1(b). In particular, the first circle in contact with the drum is reinforced with long sandstone blocks laid transversely. Big oak beams (*catene di quercia*) tie the ribs, which are entirely built of gray and tan sandstone. Therefore, even if the cupola is mainly constructed out of brick, lighter than stone and easier to form, wood, metal and stone are used where additional stiffness and strength is needed.

- *The herringbone spirals.* This technique is believed to be inherited by the Etruscans and it is documented in technical drawings dating back to the fourteenth Century [6]. As shown in Figure 2(a) for a dome of revolution, the herringbone pattern is shaped by alternating laying bricks in a horizontal way with a vertical setting at regular intervals, wider at the bottom and decreasing when going up, so to form large spirals travelling across the sections of the dome [17]. Although there is no universal agreement about the real three-dimensional disposal of the bricks [32] this arrangement, which may unfavorably overstress the sails of the membrane forming the dome, has manly a constructive purpose. In fact, the vertically laid bricks can stand up while being constrained by the horizonal ones, and further constrain the horizontally laid bricks of the successive ring against sliding on the fresh mortar. In addition, the cutting edges of the vertically laid bricks were supposedly used by a special team in charge of framing the orientation of the brickwork with a guiding cord or "trammel".

- *The radial brickwork.* Quite differently from the horizonal corbelling, the bricks of the dome, including those of the herringbone (Figure 2(b)), are all radial-oriented toward a focus point, which is "sliding" on a central axis inside the dome, as represented in Figure 3(a). There is not an unanimous agreement about the law according to which the focus should climb the central axis, but certainly, the dome was raised in successive rings [26]. If the various layers followed the radial direction of the pointed fifth arch as in Figure 3(b), the brickwork on the top would correspond to an inclination $\theta = 60°$, and the height of the focus point on the central line would be $d = 3/8\, r \tan\theta$ [15], being r the radius of point-fifth arch. The rotation of such a trammel generates a set of geometrical curves on the faceted dome surface, as shown in Figure 3(a). If that inclination toward the interior had been fixed uniquely by a single fixed central point at the bottom, the brickwork at the top would have been pushed to the very uncomfortable 90° angle, creating serious problems during construction. The internal coupling element provides the connection of the weaker parts.

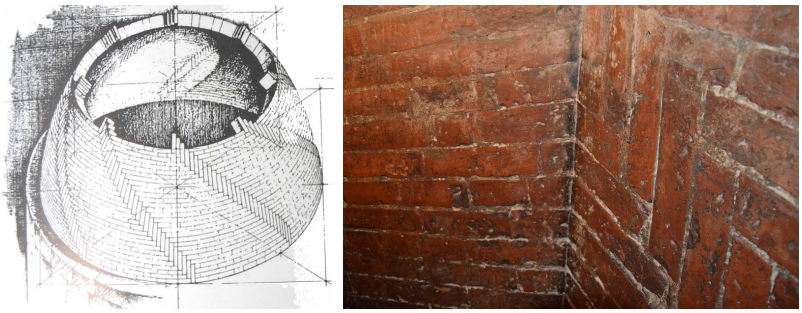

(a) (b)

Figure 2: The bond pattern of the masonry work. a) Herringbone bond pattern in a circular dome (Drawing by Francesco Gurrieri, 1982). b) Internal view of the intersection of the herringbone pattern at a corner line in Brunelleschi's octagonal-shaped dome.

The last invention in particular implies the noteworthy property that, as schematically indicated in Figure 3(c), the octagonal dome contains an invisible shell of revolution, that could be raised without falsework. Here, the inner circle corresponds to the locus of the centers of the rotating pointed-fifth arches, while C_1, C_2 and C_3 denote the intersection of the radii with the faceted dome surface in the middle of the sail or in proximity of the corner ribs, at the level of Figure 3(b). Leon Battista Alberti in his "The Ten Books of Architecture" [1], several years after the completion of the dome, gives a sense of the technique by stating" *A polygonal groin vault can also be built without centering as long as a spherical vault can be inserted into its thickness. But here you will have particular occasion for ligatures to fasten the weaker parts of the outer one tightly to the strongest part of that within*[2]. The Brunelleschi's cupola appears as a circular dome, but with parts cut away from both the inside and the outside, to leave the octagonal cloister-vault form.

It is clear from the previous discussion that the major properties of the Florentine building derive from the ingenious bond pattern set up by Brunelleschi, and that any attempt to supersede this aspect with a continuous modelling cannot but end in utter failure. Here, we propose to consider the dome as formed by rigid blocks in unilater frictional contact. Varying the shape and the bond pattern of the constituent blocks, our aim is to investigate the peculiarities of Brunelleschi's "*modo di murare*" (technique to wall up). Of course, it is impossible for our calculation potential to reproduce all structural details, and therefore a simplified model will be considered. In particular, we will not separate the dome into the two vaults coupled by ribs and rings, but we will consider an effective shell, of the same thickness of the inner vault. Parameters of comparison will be the shape of the vault (circular vs. octagonal), the bond pattern (radial vs. corbelled), and the effects of the

[2]Alberti (*De Re Aedificatoria*, liber III, Caput XIX), verbatim says: "*Angularem quoque testudinem sphericam modo per eius istius crassitudinem rectam sphericam interstruas, poteris attollere nullis armamentis. Sed istic nexura potissimum opus est, qua huius imbecillae partes partibus illius firmioribus arctissime illigentur* ". Alberti, at the begging of the same chapter, defines the various types of vaults (*testudines*), in particular the groin vault (*spherica angularis*) and the spherical vault (*recta spherica*).

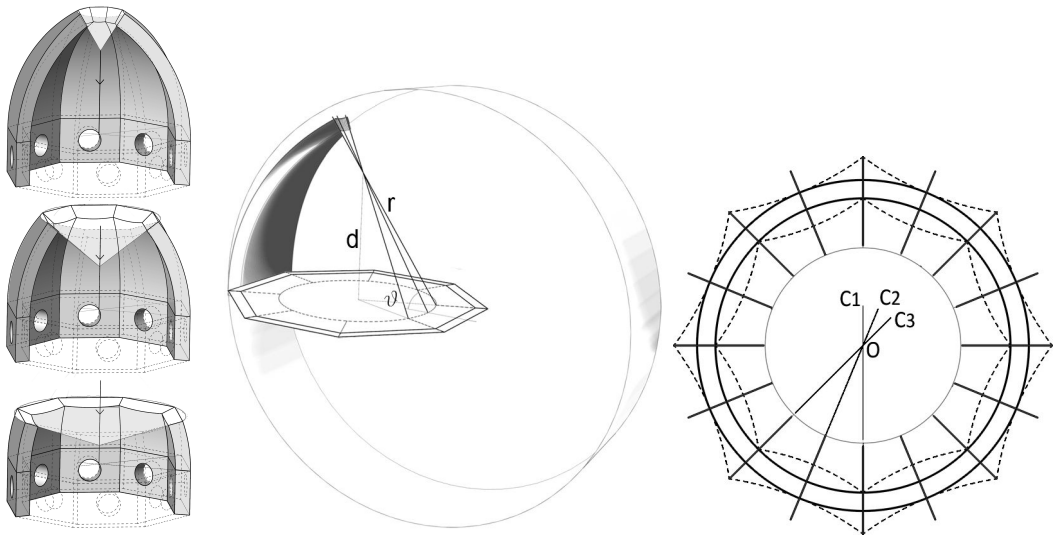

(a) (b) (c)

Figure 3: Geometry of the dome. a) Construction with auxiliary cones [6]; b) the circular construction; c) the inner, hidden, dome of revolution, inscribed in the octagonal groin vault (redrawn from the ground plan by Claudio Rossi after Lando Bartoli [6]).

1

herringbone spirals on the diffusion of the internal forces.

The frictional sliding problem for assemblies of rigid blocks is solved within the framework of Non Smooth Contact Dynamics (NSCD), according to the original formulation by J.J. Moreau [30, 31]. The blocks are considered with infinite compressive strength, subject to set-valued force laws and complementarity constraints at each contact according to frictional Coulomb's law. This model has been implemented in a custom simulator based on the Project Chrono C++ software library, interfaced with the Rhino CAD environment using the Grasshopper parametric design software. The major potentialities of the model and its numerical implementation, which includes a sophisticated contact detection algorithm, have been presented in [7]. Other authors [13, 34, 28] have instead used, as an alternative, the LMGC90 software [19] that implements the same general model, but here we prefer to use our own code with a customized procedure that can be tailored for the case at hand.

The Project Chrono software has been successfully employed in [9] to evidence the role of friction on the stability of masonry domes, imagined to be composed of blocks in dry contact, highlighting the role of the bond pattern and aspect ratio of the blocks on their capacity of equilibrating the hoop stress. The same approach has also been used to discuss the shear failure of single- or multi-ring arches, either isolated or with spandrels [8]. However, the problem considered now is much more complex than those considered so far, because the model is composed of a great number of blocks in contact on planar surfaces, so that the number and location of contact points is highly undetermined. Therefore, of

paramount importance is the use of a regularization procedure in the form of a numerical compliance, which enforces the uniqueness of the solution in terms of dual variables (contact reactions) and can be representative of the deformation of the mortar joints between the blocks. This technique is complementary to the introduction of a regularization term that, as discussed at length in [8], annihilates at each time-step the shear-induced dilatation consequent to the associative version of the frictional model used in the numerical solution. This formulation increases the numerical efficiency, it is in agreement with experiments on dry joints [38, 12, 11] and implies that the frictional response becomes non-associative as the dilatations progress.

In this article we test in a very challenging and complex problem the efficiency of the customized implementation of the NSCD approach, to demonstrate that it can be a very powerful tool to analyze masonry works for which the bond pattern and the shape of the bricks represent the *raisons d'être* of their load bearing capacity. This is why, in Section 2, the implemented model is discussed in detail, with particular emphasis on the regularization procedure that allows to determine the contact forces. On the other hand, the careful numerical experiments, recorded in Section 3, undisclose aspects of the Brunelleschi masterpiece that, to our knowledge, have only been qualitatively appreciated so far. The analysis of the flow of the contact forces and the comparison with the results for a dome of revolution with a radial brickwork and for an octagonal groin vault with corbelled construction, have evidenced the role of the hidden, circular dome ingeniously conceived by Brunelleschi. Of particular interest is the discussion about the herrigbone spirals, which are stiffer than the rest of the masonry with respect to meridional actions so to induce a strong disturbance in the flow of stress, but are more prone to open under the effects of the hoop tensile stress. Therefore, they represent the Achilles heel in the construction, as confirmed by the cracks that are visible at the points where the plaster has detached.

2 The Non-Smooth-Contact-Dynamics (NSCD) model

The NSCD formulation is typically used to describe the dynamic interaction of a large number of rigid bodies, especially of spherical shape, in frictional unilateral contact. A classical application is in the simulation of bodies impinging on layers of granular materials, while the specialization of this technique to the case of complex masonry-like construction is yet to be fully appreciated, since it presents challenging problems. First of all, the blocks are usually defined by planar surfaces, so that the location of the contact points is highly undetermined. Secondly, since some of the blocks may be non-convex, standard contact-detection algorithms cannot be readily applied. Most of all, since here we mainly perform static analyses (displacements and velocities are small), it is important to realize the advantages and drawbacks of the method and propose efficient regularization procedures that can also serve to model the deformability of the mortar joints. After recalling the main features of the NSCD model, for which we mainly refer to previous work [7], we will focus on these aspects.

2.1 The dynamical problem and its numerical implementation

The NSCD approach relaxes some limiting assumptions of ordinary differential equations, leading to a problem of measure differential inclusions (MDI) [31, 30]. The non-smooth nature of the problem stems from the fact that contact forces are assumed as set-valued force laws [36], and by accepting discontinuities in speeds as a consequence of hard contacts.

With respect to an inertial reference system, let $\boldsymbol{x}_j \in \mathbb{R}^3$ represent the position of the center of mass of the $j-$th block, $\boldsymbol{\rho}_j \in \mathbb{H}_1$ its rotation expressed as a unit-quaternion, $\dot{\boldsymbol{x}}_j \in \mathbb{R}^3$ its velocity and $\boldsymbol{\omega}_j \in \mathbb{R}^3$ the angular velocity, respectively. The state of the system at time t is represented by generalized configuration coordinates $\boldsymbol{q} = \{\boldsymbol{x}_1^T, \boldsymbol{x}_2^T, ...\}^T$ and by the generalized velocities $\boldsymbol{v} = \{\dot{\boldsymbol{x}}_1^T, \boldsymbol{\omega}_1^T, \dot{\boldsymbol{x}}_2^T, \boldsymbol{\omega}_2^T, ...\}^T \in \mathbb{R}^{n_v}$. In the MDI context, speeds $\boldsymbol{v}(t)$ are *functions of Bounded Variation* [2] in order to accommodate impulsive events in hard contacts, and positions $\boldsymbol{q}(t)$ are absolutely continuous functions with respect to the Lebesgue measure of time.

We define the set $\mathcal{G}_\mathcal{A}$ of contact constraints between pairs of shapes through a signed distance function so that the non-interpenetration condition for the $i-$th contact is $\Phi_i(\boldsymbol{q}) \geq 0$. The set $\mathcal{G}_\mathcal{A}$ is updated during the simulation by the *collision detection engine*, which adds, removes or updates contacts at each time step. At the $i-$th contact point of each block a local *contact coordinate system* is defined by a normal unit vector and two mutually orthogonal tangent vectors. The $i-$th relative velocity $\boldsymbol{u}_i = \{u_{n,i}, u_{u,i}, u_{v,i}\}^T$ is the difference between the instantaneous velocity of the near particles of the blocks at hand, expressed in the contact coordinate system. This is related with generalized velocities as $\boldsymbol{u}_i = D_i^T \boldsymbol{v}$, with matrices $D_i \in \mathbb{R}^{n_v \times 3}$. The $i-$th contact force, expressed in the contact coordinate system, is $\widehat{\boldsymbol{\gamma}}_i = \{\widehat{\gamma}_{n,i}, \widehat{\gamma}_{u,i}, \widehat{\gamma}_{v,i}\}^T$. This corresponds to a generalized contact force $D_i \widehat{\boldsymbol{\gamma}}_i$.

Using the the De Saxcé bipotential [36] on active contacts (with $\Phi_i = 0$), the three-dimensional Coulomb-Amontons frictional contact model can be expressed as a Cone Complementarity Problem (CCP)[3]. Introducing the second order Lorentz cones

$$\Upsilon_i = \left\{ \widehat{\gamma}_{n,i}, \widehat{\gamma}_{u,i}, \widehat{\gamma}_{v,i} \mid \mu \widehat{\gamma}_{n,i} \geq \sqrt{\widehat{\gamma}_{u,i}^2 + \widehat{\gamma}_{v,i}^2} \right\} \quad \subset \mathbb{R}^3 \,, \tag{3}$$

and their dual cones $\Upsilon_i^* = \{\boldsymbol{y}_i | \, \langle \boldsymbol{y}_i, \boldsymbol{x} \rangle \geq 0, \quad \forall \boldsymbol{x} \in \Upsilon_i\}$, the condition that enforces the Coulomb-Amontons contact model is the CCP defined as

$$\widehat{\boldsymbol{\gamma}}_i \in \Upsilon_i \perp \bar{\boldsymbol{u}}_i \in \Upsilon_i^* \,, \quad \forall i \in \{\mathcal{G}_\mathcal{A}, \Phi_i = 0\} \,, \tag{4}$$

[3]The *dual cone* $\mathcal{K}^*$ of the cone $\mathcal{K}$ is a convex cone expressed as

$$\mathcal{K}^* = \{\boldsymbol{y} \in \mathbb{R}^n : \langle \boldsymbol{y}, \boldsymbol{x} \rangle \geq 0 \quad \forall \boldsymbol{x} \in \mathcal{K}\} \,. \tag{1}$$

A *Cone Complementarity Problem* $\mathrm{CCP}(A, \boldsymbol{b}, \Upsilon)$ is the problem of finding a $\boldsymbol{x}$ that satisfies

$$A\boldsymbol{x} - \boldsymbol{b} \in \Upsilon^*, \quad \boldsymbol{x} \in \Upsilon, \quad \langle A\boldsymbol{x} - \boldsymbol{b}, \boldsymbol{x} \rangle = 0, \tag{2}$$

where Υ is a (convex) cone. One can also use the notation $A\boldsymbol{x} - \boldsymbol{b} \in \Upsilon^* \perp \boldsymbol{x} \in \Upsilon$. The CCP is equivalent to a Variational Inequality problem.

where we have defined

$$\widehat{\boldsymbol{\gamma}}_i = \left\{ \begin{array}{c} \widehat{\gamma}_{n,i} \\ \widehat{\gamma}_{u,i} \\ \widehat{\gamma}_{v,i} \end{array} \right\}, \quad \bar{\boldsymbol{u}}_i = \left\{ \begin{array}{c} u_{n,i} \\ u_{u,i} \\ u_{v,i} \end{array} \right\} + \left\{ \begin{array}{c} \mu\sqrt{u_{u,i}^2 + u_{v,i}^2} \\ 0 \\ 0 \end{array} \right\} = \boldsymbol{u}_i + \tilde{\boldsymbol{u}}_i \,. \tag{5}$$

The CCP above satisfies at once the requirement that contact forces reside in the Coulomb friction cone if in sticking state, and that the sliding velocity is opposite to the tangential contact force if sliding. At the same time, it implies also that no interpenetration can happen in case of contact, as the Signorini complementarity condition expressed at the speed level [7, 8].

Let now $\boldsymbol{f}(\boldsymbol{q}, \boldsymbol{v}, t)$ denote the generalized forces, including gravitational forces, external applied forces, gyroscopic forces. The block-diagonal mass matrix M contains all the masses and inertia tensors of the rigid bodies. The equilibrium condition for all the blocks is the MDI problem defined as

$$M\frac{d\boldsymbol{v}}{dt} = \boldsymbol{f}(\boldsymbol{q}, \boldsymbol{v}, t) + \sum_{i \in \mathcal{G}_\mathcal{A}} D_i \widehat{\boldsymbol{\gamma}}_i(t) \,, \tag{6}$$

$$\widehat{\boldsymbol{\gamma}}_i \in \Upsilon_i \perp \bar{\boldsymbol{u}}_i \in \Upsilon_i^* \quad \forall i \in \{\mathcal{G}_\mathcal{A} | \Phi_i = 0\} \,. \tag{7}$$

A practical approach to perform the time integration is based on a discretization of (6)-(7) at the speed level. The unknowns are the jumps in discontinuous velocities $(\boldsymbol{v}^{(l+1)} - \boldsymbol{v}^{(l)})$ over a time step h and reaction impulses $\boldsymbol{\gamma}_i = \int_t^{t+h} d\boldsymbol{\gamma}_i(dt)$. The signed Radon measure $d\boldsymbol{\gamma}_i$ can be decomposed as $d\boldsymbol{\gamma}_i = \widehat{\boldsymbol{\gamma}}_i(t)dt + \boldsymbol{\xi}_i$, where $\widehat{\boldsymbol{\gamma}}_i(t) \in L^1$ is the absolutely continuous part with respect to the Lebesgue measures dt, while the atomic measures $\boldsymbol{\xi}_i$ generates instantaneous changes in velocity.

Of paramount importance in this formulation is the introduction of a stabilization term $\boldsymbol{b}_i$ at each $i-$th contact point, which modifies the relative velocity $\bar{\boldsymbol{u}}_i^{(l+1)}$ as

$$\underline{\bar{\boldsymbol{u}}}_i^{(l+1)} = \bar{\boldsymbol{u}}_i^{(l+1)} + \boldsymbol{b}_i \,, \quad \text{with } \boldsymbol{b}_i = \{\Phi_i/h, 0, 0\} \,. \tag{8}$$

This takes care of correcting interpenetration constraints caused by numerical integration errors [24, 4], but it has other major implications that will be discussed later on. In conclusion, the time stepping scheme, to be solved at each time step, is of the form

$$\boldsymbol{\gamma}_i \in \Upsilon_i \perp \underline{\bar{\boldsymbol{u}}}_i^{(l+1)} \in \Upsilon_i^* \,, \tag{9}$$

$$M^{(l)}(\boldsymbol{v}^{(l+1)} - \boldsymbol{v}^{(l)}) = h\boldsymbol{f}(\boldsymbol{q}^{(l)}, \boldsymbol{v}^{(l)}, t^{(l)}) + \sum_{i \in \mathcal{G}_\mathcal{A}} D_i \boldsymbol{\gamma}_i \,, \tag{10}$$

$$\boldsymbol{q}^{(l+1)} = \Theta(\boldsymbol{q}^{(l)}, \boldsymbol{v}^{(l+1)}) \,, \tag{11}$$

where, in (11), the Θ map performs the incremental update of coordinates. For positions it simply means $\boldsymbol{x}_i^{(l+1)} = \boldsymbol{x}_i^{(l)} + h\dot{\boldsymbol{x}}_i^{(l)}$, whereas a Lie exponential is used for updating rotations.

These conditions solve the general dynamical problem, but the same formulation can be used for static analysis as a special case. A static analysis can be achieved with a single solution of the CCP with arbitrary h and with $\boldsymbol{v}^{(l)} = \mathbf{0}$, a highly non-linear complementarity problem whose solution gives $\boldsymbol{v}^{(l+1)}$ and contact forces $h\boldsymbol{\gamma}$. Unstable configurations would correspond to non-zero $\boldsymbol{v}^{(l)}$. We remark that, in the context of finite precision as happens on most computer implementations, the solution of the CCP would give anyway a non-zero $\boldsymbol{v}^{(l)}$ even if the configuration is stable, hence a tolerance ϵ_s would be needed. When approaching unstable configurations, the definition of a proper tolerance can be questionable, so we prefer to perform full dynamic analysis, with a duration of 4 s, even for the assessment of the stability.

2.2 Solution and regularization of the problem

The main computational bottleneck of the time stepping scheme is the computation of unknown impulses $\boldsymbol{\gamma}$ from the CCP of (9). For its practical implementation, we introduce system-level matrices and vectors $D = [D_1 \mid ... \mid D_{n_\mathcal{A}}]$, $\boldsymbol{\gamma} = [\boldsymbol{\gamma}_1 \mid ... \mid \boldsymbol{\gamma}_{n_\mathcal{A}}]$, $\bar{\boldsymbol{u}} = [\bar{\boldsymbol{u}}_1 \mid ... \mid \bar{\boldsymbol{u}}_{n_\mathcal{A}}]$, $\boldsymbol{b} = [\boldsymbol{b}_1 \mid ... \mid \boldsymbol{b}_{n_\mathcal{A}}]$, and the Cartesian product of all friction cones $\Upsilon = \times_{i\in\mathcal{G}_\mathcal{A}}\Upsilon_i$, $\Upsilon^* = \times_{i\in\mathcal{G}_\mathcal{A}}\Upsilon_i^*$, where $n_\mathcal{A}$ denotes the number of contacts. Also, for compactness we write $\tilde{\boldsymbol{k}}^{(l)} = M^{(l)}\boldsymbol{v}^{(l)} + h\boldsymbol{f}_t(\boldsymbol{q}^{(l)}, \boldsymbol{v}^{(l)}, t^{(l)})$. Finally, having defined the Delassus operator $N = D^T {M^{(l)}}^{-1} D$ and the vector $\boldsymbol{r} = D^T {M^{(l)}}^{-1}\tilde{\boldsymbol{k}} + \boldsymbol{b}$, we can rewrite (9) as a non-linear second-order CCP in the form

$$\boldsymbol{\gamma} \in \Upsilon \perp \left(\underline{\bar{\boldsymbol{u}}} = N\boldsymbol{\gamma} + \boldsymbol{r} + \tilde{\boldsymbol{u}}(\boldsymbol{v}^{(l+1)})\right) \in \Upsilon^* . \tag{12}$$

A first difficulty in solving (12) is the presence of the non-linear $\tilde{\boldsymbol{u}}(\boldsymbol{v}^{(l+1)})$ term. It has been shown [5] that under the assumption of small time steps and/or small sliding speeds, such term can be dropped in order to obtain an easier convex problem, with affine $\underline{\bar{\boldsymbol{u}}} = N\boldsymbol{\gamma} + \boldsymbol{r}$. After such a convexification, the CCP can be cast as a quadratic program with cone constraints, a class of optimization problems for which we can use an efficient solver. To this end we developed a variant of the non-monotone Spectral Projected Gradient method with non-monotone Grippo-Lampariello-Lucidi line search [10], adding diagonal preconditioning and a fall-back strategy to ensure monotone convergence in truncated iterations. We experienced that in most scenarios this method converges faster than fixed point iterative solvers usually adopted in earlier NSCD algorithms [23].

A drawback of the convexification is that the Coulomb friction model becomes associative as a dilatation is generated during sliding motion. However, such a dilatation does not increase indefinitely, because of the stabilization term $\mathbf{b}$ defined in (8). This implies that during sliding motion the gap tends to $h\mu\sqrt{u_{u,i}^2 + u_{v,i}^2}$ and, as such, it becomes irrelevant

for small time steps or small sliding speeds like in the original non-associative Coulomb model [3, 5]. A detailed discussion of this effect is recorded in [8].

A second difficulty emerges from the fact that existence and uniqueness of the solution to the CCP problem holds in the static regime only under special circumstances [7]. It is sufficient to take the counter-example of a rigid tripod stacked on top of a plane, at rest, for which there are infinitely many solutions for the tangential reactions at the three contact point, provided that they cancel out in horizontal direction. Adding further contact points between two rigid bodies leads to even more over-constrained problems. Although multiple solutions for contact reactions (dual variables) might correspond to an unique solution in terms of speeds (primal variables), hence not causing issues in plotting trajectories, this remains a problem if one desires to visualize the flow of forces inside in a masonry work. For instance, at each time step the CCP solver may converge to a different solution in terms of dual variables even if the blocks show little or no motion, which triggers a noisy display of contact forces that seems to cycle between different solution sets. In addition, over-constrained problems, like those considered later on, are very sensitive to the initial boundary conditions.

For the reasons above, we introduce a regularization in the form of a numerical compliance in contacts. In [37] we introduced the stiffness matrices K_i, at each i-th contact, with $k_{n,i}$, $k_{u,i}$, $k_{v,i}$ values on the diagonal; we arranged them in a single system-level block-diagonal matrix K and demonstrated that the only modification required to the original NSCD time stepping is the introduction of a block diagonal E matrix in the Delassus operator, i.e.,

$$N \;=\; D^T {M^{(l)}}^{-1} D - E\,, \tag{13}$$

with $E = -\frac{1}{h^2}K^{-1}$. One can see that for $k \to \infty$, this model converges to the original scheme. Although our method aims at using large time steps h for high computational performance, in passing we note that for $h \downarrow 0$ the method tends to an explicit integrator where the $D^T {M^{(l)}}^{-1} D$ part becomes less and less relevant. If damping is required too, we can add a stiffness-proportional damping $R_i = \alpha K_i$ at each i-th contact, leading to $E = -\frac{1}{h(h+\alpha)}K^{-1}$. In such a case, anyway, also the $\boldsymbol{b}_i$ terms of (8) shall be modified, becoming $\boldsymbol{b}_i = \{\frac{1}{h+\alpha}\Phi_i, 0, 0\}$. Tuning a proper damping value can be useful for simulation involving seismic scenarios, but in our case, that is addressing a static problem, the damping can be neglected; moreover, the time stepping itself already introduces a numerical damping which grows with the size of the time step, as in a first order implicit integrator.

However, one can see from (8) that $\boldsymbol{b}_i$ contains a term that is proportional to $\frac{1}{h}$, and this can be a problem for simulations using small time steps together with small (or zero) compliance. In such cases, the algorithm tends to cancel possible penetrations in a single step, thus giving residual outbound speeds at the next time step. Such artefact can affect the numerical stability of simulations, because stacked objects tend to bounce instead of settle. In order to control this numerical issue, we introduce an optional numerical tolerance

ϵ_u that enforces and upper limit on the speed of recovery of penetrations. Then, the $\boldsymbol{b}_i$ terms become, in the various cases,

$$\boldsymbol{b}_i = \left\{ \max\left(\frac{1}{h}\Phi_i, \epsilon_u \right), 0, 0 \right\} \quad \text{rigid or compliance}\,, \tag{14}$$

$$\boldsymbol{b}_i = \left\{ \max\left(\frac{1}{(h+\alpha)}\Phi_i, \epsilon_u \right), 0, 0 \right\} \quad \text{compliance and damping}\,. \tag{15}$$

The ϵ_u contribution can be interpreted as an additional numerical damping in contacts, which is automatically triggered only when needed.

A consequence of having introduced E is that the N matrix, which was originally positive-semidefinite because of the high rank-deficiency of D, becomes a positive-definite matrix. Thanks to this, we get the uniqueness of the solution for the dual variables, so that the solver converges stably to the same solution in terms of dual variable at each timestep. This is different from a penalty approach because it still fits in the variational formalism for non-smooth set-valued forces and, hence, the time integration algorithm retains a good stability even when taking large time steps.

This compliance is a departure from the original idea of perfectly rigid blocks, but it can be exploited to model the deformability of the mortar joints between the stone or masonry blocks. As noted in [25], one may want to apply physical compliance values that match the stiffness of the real materials. However, we will show that a precise evaluation of this effect is not crucial, because the distribution and value of the contact forces is almost insensitive to the assumed value of the compliance, at least in a certain significant range. Extremely small values, even without physical meaning, will make N positive-definite anyway, providing uniqueness of $\boldsymbol{\gamma}$ solutions. In general our numerical experiments have demonstrated that lower compliance parameters lead to faster convergence of the iterative solver.

2.3 Collision pipeline

Masonry structures contain thousands of blocks, some of them not even convex; this calls for advanced collision detection algorithms [27]. Computing the set $\mathcal{G}_\mathcal{A}$ of contact points for all possible pairs of shapes would lead to an algorithm with $O(n^2)$ complexity class. Because of this, our collision pipeline is split in two phases: a fast *broad phase*, which sorts out only those pairs of blocks whose bounding box is overlapping, and a successive *narrow phase*, which focuses on those pairs, by refining one or more contact points between them. For the broad phase filtering we use a bounding volume hierarchy based on a dynamic tree of Axis Aligned Bounding Boxes as implemented in [16]. The narrow phase stage operates on the pairs of blocks being selected by the previous broad phase. The implemented method relies upon the Gilbert-Johnson-Keerthi (GJK) algorithm [20], that returns a couple of nearest points between a pair of *convex* shapes. The GJK algorithm is fast and operates

on whatever kind of convex surface (boxes, faceted polytopes, cylinders, etc.), but there are three issues to be addressed.

The first problem comes from the fact that the GJK algorithm assumes shapes to be separated, but the time integration might not be able to prevent slight interpenetration between some blocks. To overcome this issue, as shown in Figure 4(a) we regularize the original shapes as sphere-swept surfaces, i.e., smaller shapes with rounded corners with radius ϵ_m, and then the GJK algorithm is run on the smaller, shrunk shapes. This idea significantly enhances the robustness of the collision pipeline. Referring to Figure 4(b), when the nearest contact points P'_A and P'_B are found between the shrunk shapes, we offset them along the normal by a quantity ϵ_m, to obtain P_A and P_B, that are sent to the $\mathcal{G}_A$ set. In this way, the multibody solver operates on P_A and P_B, rather than on P'_A and P'_B. In other words, we accept penetrations with negative distance up to $2\epsilon_m$ between P_A and P_B, while P'_A and P'_B are still separated with positive distance. The pre-processing of the original shapes of the blocks to generate the inset shrunk shapes is done with the algorithm suggested in [33]. A side effect of this workaround is that original sharp edges behave as rounded by a fillet of radius ϵ_m; however this is not a real problem for blocks used in architectural construction, which never present perfectly sharp corners.

A second difficulty is represented by the fact that most contacts are degenerate cases where two faces are coplanar as in 4(c). This indeterminacy is here solved by running the GJK algorithm multiple times with small perturbations on object rotations, thus obtaining candidate contacts in multiple positions. Then, an heuristic collision filtering step discards unnecessary contacts by keeping only a limited set of them, namely those that maximize the contact patch. The introduced perturbations may raise a disturbance in the flow of contact forces, which are enhanced by the fact that the problem is highly non-linear. In particular the solution in terms of contact forces may slightly deviate from the perfect symmetry expected from geometry and applied loads. However, the disturbance is limited and, in case, it may be representative of the inevitable construction tolerances for a real case.

A third issue comes from fact that in a complex stereotomy there are blocks that are non-convex, whereas the GJK algorithm operates on convex shapes only. This difficulty is bypassed by performing a convex decomposition of concave shapes into multiple polytopes during a pre-processing phase. This done, the GJK algorithm can operate on the single (convex) sub-blocks contained in a single rigid body. A drawback of this approach is that the amount of generated contacts between pairs of concave shapes can be quite high; moreover such amount depends on the level of detail used in performing the convex decomposition of concave blocks. In fact, different decomposition algorithms can produce different amounts of contacts even for the same shapes. This can be an issue when using regularization in contacts, as the overall compliance of the mating will depend on the number of contacts created between the two surfaces, for the same stiffness values $k_{n,i}$, $k_{u,i}$, $k_{v,i}$ assigned to single contacts. To avoid this indeterminacy we performed the convex decomposition with an ad-hoc algorithm that generates uniform radial slices of non-convex blocks like those of Figure 4(d), which are typical for a domed structure.

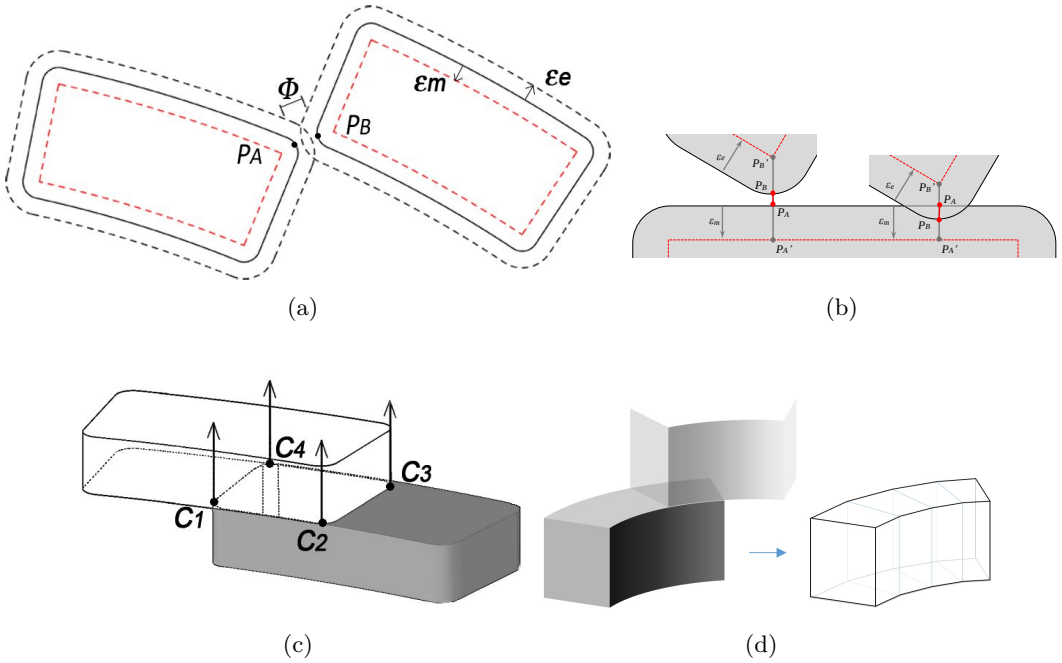

(a) (b) (c) (d)

Figure 4: Treatment of the blocks in contact. a) Collision shapes and tolerances; b) Robust handling of small penetrations using sphere-swept surfaces; c) Multiple contact points between coplanar facets; d) Convex decomposition of a concave block into multiple convex polytopes via radial slicing.

3 Numerical experiments

After having defined the general layout of the model, we consider various arrangements of the brickwork, differing in the shape of the vault (circular vs. octagonal), the bond pattern (radial vs. planar), and the possible presence of the herringbone spirals.

3.1 Geometry and material properties

For an estimated weight of about 37000 tons, the *cupola* with (without) the lantern is 116 m (91 m) high, while the internal (external) diameter is about 45 m (54 m) at the drum level at 54 m height. The proposed model is relatively simple, since we do not consider the coupled double-shell and we limit to analyze the response of one shell of effective constant thickness equal to 2.2 m, whose inner surface coincides with the intradox of the real dome and follows therefore the characteristic profile of the *quinto acuto*. The number of blocks is constant at each ring so that their width varies with the height: apart some blocks slightly ($\sim 1/4$) smaller or larger than the others in order to avoid collinear vertical joints, the average size of the blocks is $b \times s \times h = 4.5 \times 2.2 \times 1$ m^3 at the base, and $1 \times 2.2 \times 1$ m^3 at

the top. In general, the bricks are laid in radial direction, following the conical construction already anticipated in Figure 3. In particular, the contact layers along the parallels at each ring are obtained by rotating the radius of the *quinto acuto* arch at that level around the central axis of the dome, so that the locus of the centers is the inner circle drawn with light continuous line in Figure 3(c). The various models are composed of approximately 1300 blocks in unilateral frictional contact.

This construction is repeated also for the herringbone spirals, giving rise to a quite complex bond pattern. In the real dome, the number of herringbones is ten for each sail, i.e., they are posed at a distance of about 1.8 m one from the other in proximity of the base, but here we simplify this geometry by considering just one herringbone per sail, consistently with the assumed size of the blocks. Horizontal sections of the dome at 14.5 m and 22.5 m over the impost, are reported in Figures 5(a) and 5(b), respectively. From this it is evident that, although the dome is composed by a single layer of bricks, the conical construction and in particular the inclination of the bed joints at each ring (Figure 3) is such that a *horizontal* radial segment may intercept more than one block. Remarkably, these sections highlight the "hidden" circular dome referred to in Figure 3(c). Vertical Sections of the dome at the two stages of constructions at 14.5 m and 22.5 m are reported in Figures 5(c) and 5(d). It should be noted here that most blocks result to be non-convex, so that the special algorithm for contact detection described in Section 2.3 needs to be applied.

The specific weight of the material is set equal to 18 kN/m^3, and the friction coefficient is kept fixed to $\mu = 0.4$ in all the numerical experiments. An important material parameter, which is associated with the compliance of the mortar joints, is represented by the diagonal matrix E of eq. (13), whose terms are all set equal to 10^{-8} m/N to define the normal and tangential compliance at each contact point. Taking into account the order of magnitude of the reaction contact forces at the single point and the weight of the dome, this implies a displacement associated with the compliance of the order of $15 - 20$ mm for the blocks at the base of the dome. Such a value should be associated with the deformation of all the mortar joints of the assembly of bricks that each block of the model ideally represents. The bricks of the real dome have sizes varying from $b \times s \times h = 34 \times 17 \times 5$ cm^3 to $44 \times 22 \times 5$ cm^3 [14], so that the constituent rigid bodies of the model are indeed macroblocks equivalent to assemblies of about 2000 bricks. This simplification is crucial for the numerical handling of the problem, but it follows that each macroblock, approximately 1 m high, contains about 20 horizontal mortar joints: the assumed compliance is associated with a settlement of the order of 1 mm for each mortar layer in the most stressed regions.

Certainly the "percolation" of contact forces in the brickwork may be affected by the assumed discretization. Although a detailed analysis of this aspect goes beyond the scope of the article, aiming at a qualitative comparison of different-in-type bond patterns for the dome, we have preliminarily studied the response of a single wall under uniaxial compression. In particular, we have considered a 12 m $\times$ 6 m wall (thickness = 1 m), under the action of the self weight (density of the blocks equal to 1800 kg/m^3) and of a uniformly distributed load at the top, equal in total to ten times the weight of the whole wall. This represents

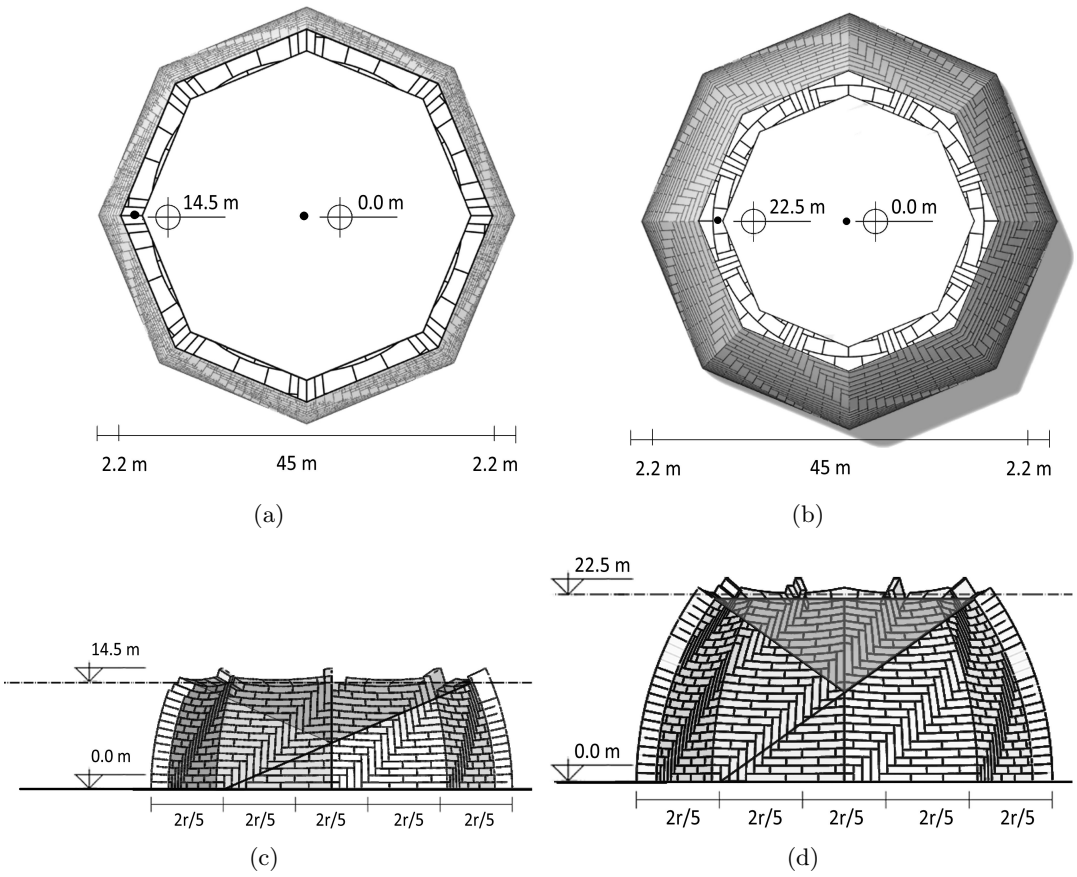

Figure 5: Construction of the model. a-b) Horizontal sections of the *complete* model at 14.5 m and 22.5 m over the impost. c-d) Sections of the *partial* model at two different levels of construction (14.5 m and 22.5 m over the impost).

a theoretical case where the blocks are almost uniformly compressed. Three different bond patterns have been considered, composed of blocks with the same aspect ratio (4:1) but different size (*large*: 6 m × 1.5 m; *medium*: 1.2 m × 0.3 m; *small*: 0.24 ×m 0.06 m). The width of the wall is maintained equal to 1 m in all the cases, in order to evidence the effects of the in-plane discretization. Various numerical experiments have been conducted for different values of the compliance matrix E of (13), varying in the range from 10^{-12} m/N to 10^{-8} m/N.

In all the considered cases, the contact forces were found to be homogenously distributed, as expected due to symmetry of the problem. Concerning the gross stiffness of the wall, associated with the displacement of the top row of blocks, this was certainly affected by the value of the compliance, but showed a mild dependence on the discretization, at least for the large and medium blocks (the small-size blocks showed numerical instabilities due to the huge number of contacts for low compliances). It should be recalled that the as-

sumed compliance acts at the level of each single contact point and, therefore, there are clearly two contrasting effects. On the one hand, an increase of the number of horizontal layers increases the number of compliances in series and, consequently, the deformability of the whole wall. On the other hand, an increase of the number of bricks forming each row increases the number of contact points on the horizontal interfaces: the increase of the number of compliances in parallel augments the stiffness of the wall. The considered numerical experiments indicate that the aforementioned two effects approximately compensate one another, at least for the large and middle size discretization, since the aspect ratio of the blocks is maintained fixed. In fact, the order of magnitude of the in-plane deformation of the wall is only mildly affected by the size of the blocks, being proportional to the assumed compliance of the contacts. Since the static state of the dome is basically governed by the gross stiffness of the constituent masonry walls, we believe that the results we obtain, albeit the discretization is coarse, are consistent at the qualitative level, so to render meaningful the comparison among different bond patters formed by blocks with similar shape and size.

In all the simulations, we never consider the effects of external environmental actions, likewise wind or thermal variations, supposing that the dead weight is the main load. The base of the dome is in contact with the horizonal plane with the same friction coefficient used for the inter-block interaction. This is equivalent to assume that the drum is not deformable, a hypothesis that is hardly verified in the real case. On the one hand, in the model we neglect that the first rings of the cupola are made with strong stone reinforced with blocks laid transversally, as well as the presence of the big oak beams, which act as confining ties equilibrating part of the hoop stress while reducing the outward radial displacement at the base [32]. Consideration of all these effects goes well beyond the scope of the present article, which is limited to a theoretical discussion of the effects of the shape and bond pattern on structural stability.

3.2 Polygonal vaults

In order to initiate the analysis, consider first octagonal vaults without the herringbone spirals, where the blocks are arranged in two different manners, either maintaining planar the bed joints of each ring composing the eight sails (*planar construction*) or following the scheme of Figures 5 (*circular construction*). Of course, in the planar construction non-convex blocks of particular shape need to be used to form the ribs at the intersection between adjacent sails, otherwise they would not be connected one another[4]. Figures 6(a) and 6(b), evidence, at three section levels, the contact forces between adjacent rings for the

[4]This is one of the first interpretations of the construction method used by Brunelleschi [35], not confirmed by successive studies. The particular bricks that were supposed to be used in proximity of the ribs were referred to as "*mattoni a libro aperto*" (open-book bricks), due to the shape that could be inferred, albeit tentatively, by observing a few spots in the interior of the dome, like that of Figure 2(b), where the brickwork is not hidden by the plaster. Later studies have confirmed that what is observed are sections of rectangular-parallelepiped shaped bricks with a dihedral angle formed by two planes intersecting on a line not parallel to any of the edges of the block.

planar and the circular construction, respectively.

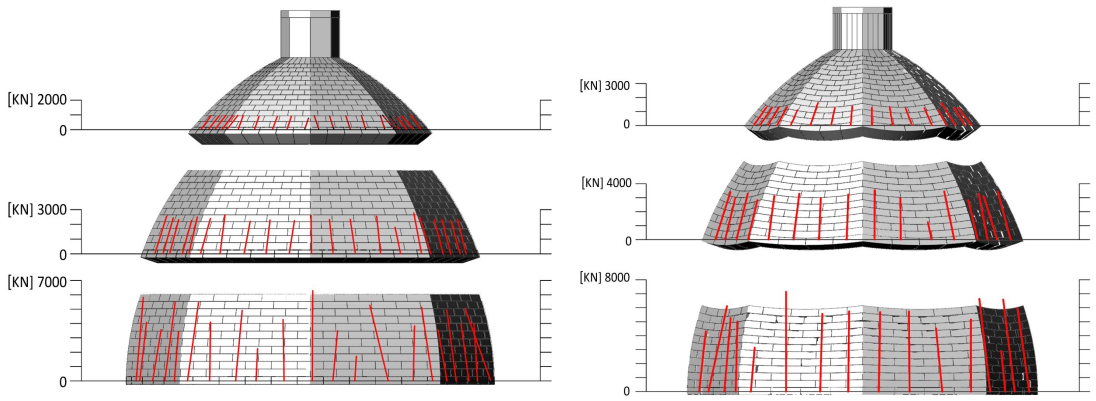

(a) (b)

Figure 6: Contact forces at three different levels for a octagonal vault. a) Planar construction. b) Circular construction.

In the most general case, a spatial system of forces is equipollent to a wrench, i.e., a force applied along a prescribed line and a couple whose moment vector is parallel to that. We have thus calculated the wrench that is equipollent to the contact forces exerted on each block by the underlying ring, and we have found that the corresponding couple is in general negligible. The length of segments reported in Figures 6 is proportional, according to the annexed measurement scale, to the force of the contact wrench. What should be noticed is that there is a considerable fluctuation of the contact forces especially at the base of the dome, which is mainly due to the highly non linear character of the problem and to the fact that most of the contacts are degenerate cases of the type of Figure 4(c). Therefore, as discussed in Section 2.2, the GJK algorithm is run multiple times with small perturbations, which on the one hand affect the regularity of the theoretical solutions, but on the other hand may be an index of the sensitivity to construction defects. In any case, albeit tentatively, from the comparison of the results in the planar and circular constructions, one can notice that the contact resultants appear more evenly distributed in the latter case, even if a certain concentration around the ribs of the vaults is appreciable. The fact that the forces in Figure 6(b) appear slightly higher than in Figure 6(a) is due to the fact that, being the stereotomy different, the dome is slightly thicker in the circular construction than in the planar construction.

Figures 7(a) and 7(b) are representative of the thrust lines for the *planar* construction along meridians that are located either in the middle of the sail or in proximity of the corner rib, respectively. Such curves are obtained by considering the envelope of the lines of the force resultants between adjacent blocks. The auxiliary graphs labelled with "r" represent, in the reference scale, the norm of the force resultant as a function of the height

of the considered ring, whereas the "v" graphs indicate the vertical component only, which is of interest to check *a posteriori* that global equilibrium is satisfied. The other auxiliary graphs in the pictures report the length, in meters, that is associated with the corresponding couple of the wrench, defined as the ratio between the moment of the couple and the force resultant. It is clear from the graphs of the second type that such lengths are in general very limited, of the order of a few centimeters, apart from the blocks at the top of the dome where they may locally reach a value of 0.4 m. This is probably due to the interaction with the weight of the lantern (set equal to 2 % of the weight of the whole dome), and the fact that at those blocks the forces of the wrench are small.

In all cases, the thrust lines remain limited inside the dome contours. The resultant of the contact forces is in practice almost linearly distributed along the height of the dome in the middle of the sail, as *per* Figure 7(a), whereas Figure 7(b) indicates a marked overloading of the rib in proximity of the base of the dome.

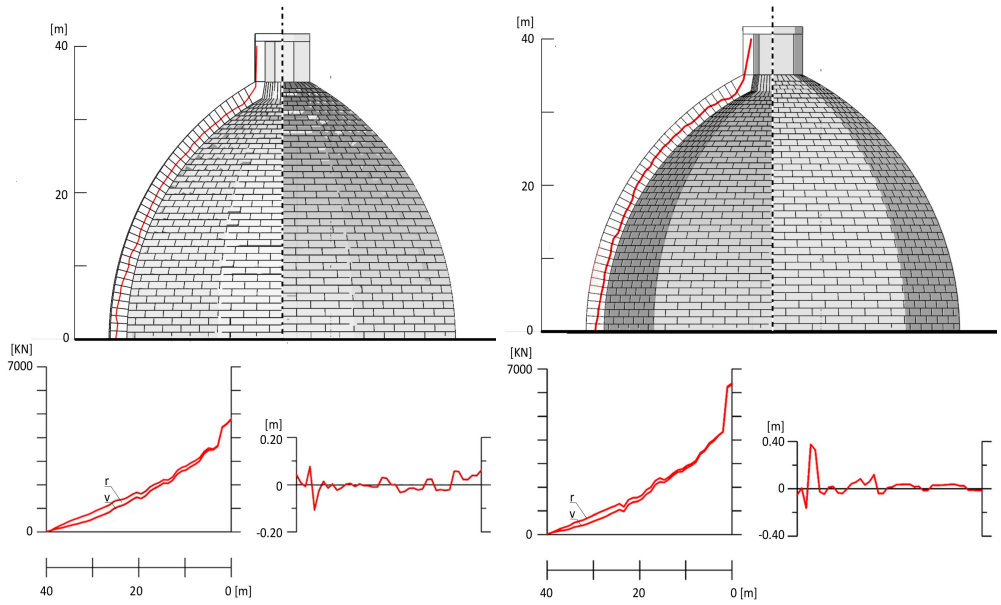

(a) (b)

Figure 7: Meridian thrust line in the octagonal vault with planar construction, with quantitative indication of the contact wrenches. a) Middle of the sail. b) Corner rib.

Figures 8(a) and 8(b) are the counterparts of the figures discussed above for the *circular* construction. Again, one can verify that the couples associated with the wrenches remain quite small. What should be noticed now is that the rib is in general more stressed than the middle of the sail, but in both cases the norm of the contact forces is in practice a linear function of the height of the dome.

In conclusion, the circular construction provides a contact flow that is slightly more

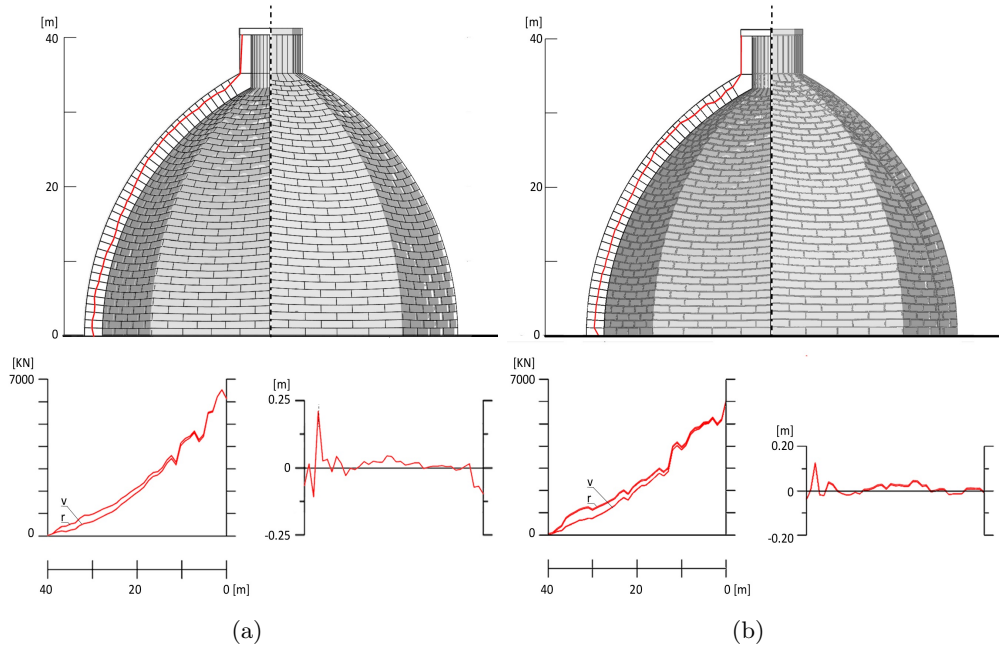

Figure 8: Meridian thrust line in the octagonal vault with circular construction, with quantitative indication of the contact wrenches. a) Middle of the sail. b) Corner rib.

evenly distributed than in the planar construction, but in general the ribs are more stressed than the middle of the sails. By insight, we may interpret the multiple use of the GJK algorithm with small imperfections, to solve the indeterminacy of multiple contact points between coplanar facets as per Figure 4(c) of Section 2.3, as an indication of possible imperfections in the block bond-pattern. Therefore, we might also conjecturally claim that the circular arrangement is less sensitive to construction tolerances.

3.3 Circular domes

The purpose here is to isolate the effects of the herringbone pattern. To do so, reference is made to the axial symmetric case of a circular dome, of course layered according to the circular construction. Figure 9(a) evidences the force resultants of the contact wrenches exerted on each block by the ring below, proportioned according to the side scale. Despite the geometric and load symmetry of the problem, we can notice that the contact reactions are not evenly distributed as one would have expected. This may be due to numerical errors, but we have verified that by varying the compliance of the mortar joints through the diagonal matrix E of (13) within the range $2 \cdot 10^{-8} \div 2 \cdot 10^{-10}$ m/N, similar results are obtained. This may be again explained with reference to the degenerate nature of the contacts, which are all of the type of Figure 4(c), and the consequent perturbation introduced by the multiple running of the the GJK algorithm. Figure 9(b) reports similar pictures when

the herringbone spirals are inserted. It is clear that these produce a disturbance in the flow of forces. In particular, the contact resultant appear higher below the herringbone arrangement, which thus plays a role somehow equivalent to a stress concentrator.

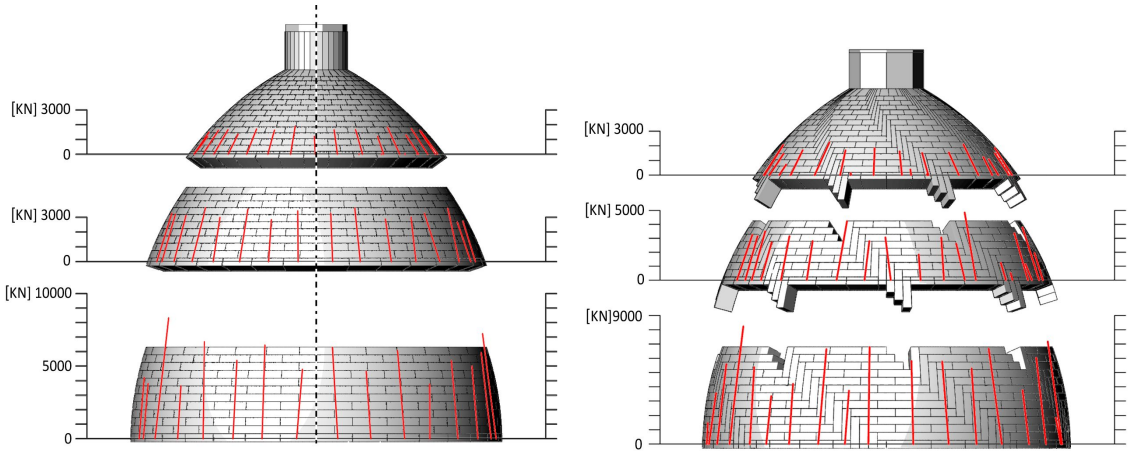

(a) (b)

Figure 9: Contact forces at different levels for a circular dome. a) Uniform bond pattern. b) With herringbone spirals.

Figures 10(a) and 10(b) represent the meridian line of thrust without the herringbone or with the herringbone, respectively, which are again well contained within the dome profile. We can notice from the auxiliary graphs of Figure 10(a) that in the *pure* circular dome the couples of the wrench are extremely limited, and the resultants are evenly distributed and follow a pseudo-linear dependence with the height of the dome. The great disturbance introduced by the herringbone spiral is evident by the comparison with Figure 10(b). The resultant of the contact forces is a wiggly function of the height of the considered parallel. It should be mentioned that the width of one standard block is three times the base of the blocks composing the herringbone, so that in this graphs we consider the resultant on three blocks when the herringbone spiral transverses the meridian. A more precise analysis of this graph indicates that the norm of the resultants of the contact wrenches is high in proximity of the herringbone. The second graph indicates that the lengths associated with the couple of the wrenches remains again well below 0.2 m, but the trend is not smooth in proximity of the herringbone.

This analysis confirms the irregular flow of forces that derives from the presence of the herringbone spirals. This effect is due to the compliances of the contact joints *via* the diagonal matrix E of (13): being the blocks rigid, this is the only source of deformation. When the blocks are laid vertically, the number of contacts that are encountered while travelling along a meridian is less than when the blocks are laid horizontally, and this is why, with respect to meridional membrane forces, the regions with the herringbone appear stiffer than the others. For a deeper discussion, Figure 11(a) reports the layout of a vertical wall

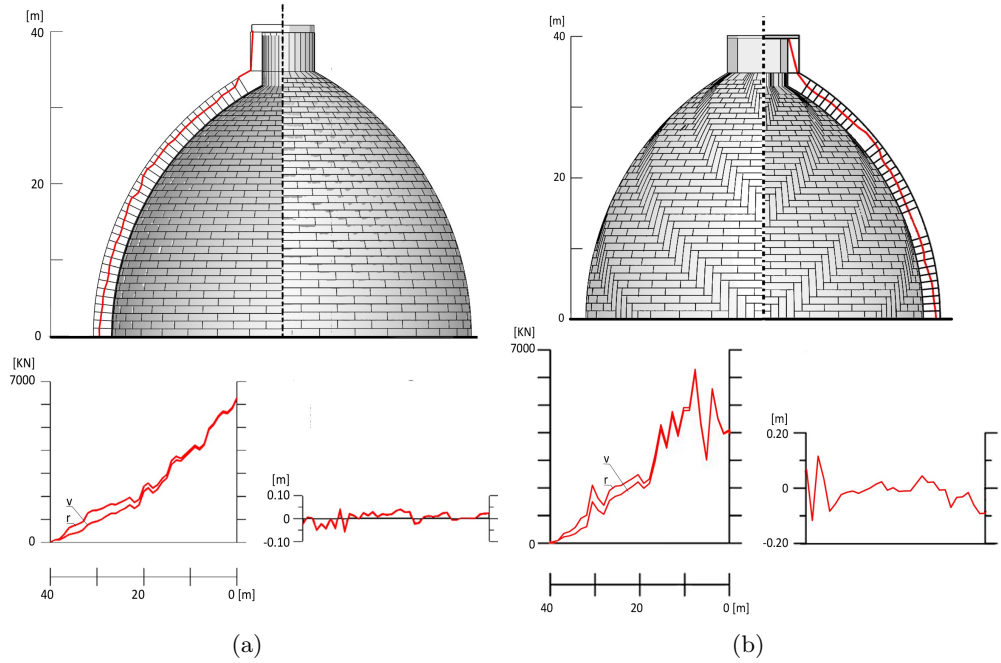

Figure 10: Meridian thrust line in the circular dome, with quantitative indication of the contact wrenches. a) Uniform bond pattern. b) With herringbone spirals.

with a herringbone diagonal, loaded by its own weight and by a uniformly distributed load on the top equal to 35% of the weight of the whole wall (block size $b \times s \times h = 4 \times 2.4 \times 1$ m^3). How the forces are distributed inside the wall is evidenced in Figure 11(b), which reports the contact reactions transmitted to each block by the portion underneath at four different heights. In proximity of the herringbone, the segment represent the resultant of the forces of the three blocks that, together, have the same width of the blocks laid horizontally.

It is clear that at the top of the walls the herringbone attracts less load than the rest of the wall, but the opposite is true at the lower layers. This is again attributed to the different vertical stiffness offered by the various columns by which the wall may be imagined to be formed, consequent to the number of compliant joints that are encountered on vertical lines. At the top of the wall, the distributed load that is carried by the vertically laid bricks is small, because small is the loaded surface. Going inside the wall, the stress diffuses and the stiffer parts carry the major load. It has been recognized by many authors [17] that the herringbone represents a disturbance in the flow of stresses, but usually it has been considered as a soft part. Here our conclusion is the opposite: the herringbone, being stiffer, becomes overstressed.

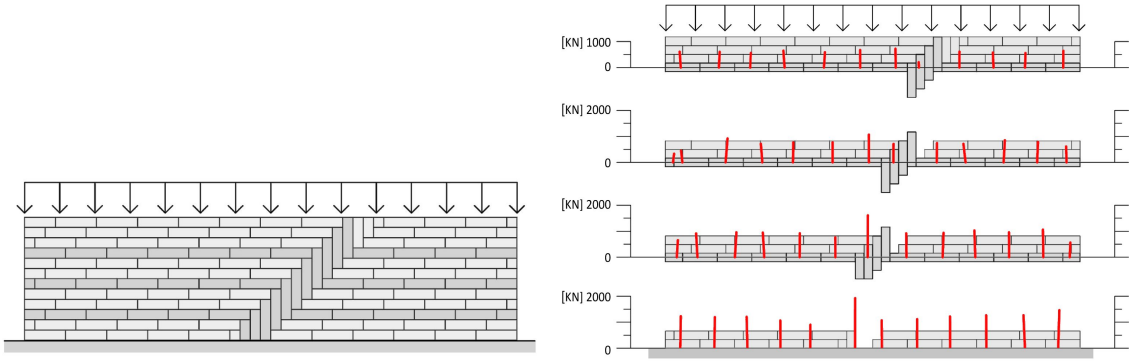

(a) (b)

Figure 11: Vertical wall with a herringbone diagonal under dead weight and uniformly distributed load (35% of the weight of the whole wall). a) Layout. b) Contact forces at various horizonal levels.

3.4 The Brunelleschi dome model

The model that is representative of the bond pattern used by Brunelleschi is the combination of the octagonal vault with circular construction of Figure 5(b) with the herringbone pattern of Figure 9(b). The force resultant of the contact wrenches are indicated at three different levels in Figure 12(a). We can notice that, as in the case of an octagonal vault, the ribs are overloaded with respect to the center of the sails, and that in general the herringbone acts as a stress concentrator. Therefore, it is not surprising that the cracks that are visible in the interior of the dome, one of which is represented in Figure 12(b), are mainly in proximity of the herringbone spirals. This fact has been also noticed in the scaled physical model constructed by Di Pasquale with micro-bricks, as mentioned in [17].

Figures 13(a) and 13(b) report the thrust line in the middle of the sails and in proximity of the ribs, respectively. Here we can again appreciate the disturbance introduced by the herrigbone, because the trend of the norm of the contact forces as a function of the height is quite irregular and jumps where the herringbone spiral transverses the meridian, resulting very similar to that of Figure 10(b) for the circular dome. The graphs of the lengths indicate again that the couple of the wrench remains limited, but it is more irregular than in the circular dome. Comparisons of the pictures referring to the middle of the sail and the rib, demonstrate that the latter is overloaded with respect to the former, a finding which is in agreement with what already discussed for octagonal vaults in Section 3.2.

The dome model does not collapse under self weight. The characterization of the *potential* kinematic mechanisms of failure under vertical loading cannot be conduced similarly to what is usually done for arches, i.e., by gradually increasing the concentrated forces that accompany the self weight [7]. In fact, either the vertical concentrated forces that are applied to a dome are very small, or particular geometries and/or additional reinforcing elements

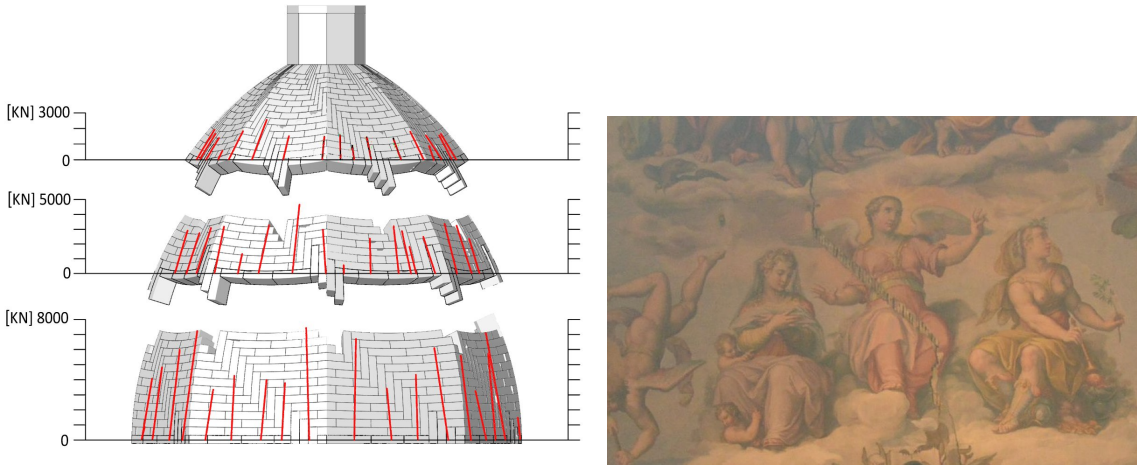

(a) (b)

Figure 12: Contact forces for the Brunelleschi dome model. a) Horizontal cuts at three different levels. b) Photograph from the interior of the dome, evidencing the fractures in proximity of the herringbone spirals

.

are explicitly conceived to take care of them. On the other hand, since the frictional shear forces are a linear function of the normal forces, a theoretical increase of the weight *per* unit volume of the dome does not produce modifications in the equilibrium state under the hypothesis of rigid blocks with infinite strength, even if a slight difference may appear due to the implemented compliance at the contact joints, as indicated in Section 2.2. Therefore, in order to evidence the possible collapse mechanisms, the friction coefficient has been gradually reduced from the value $\mu = 0.4$, used in all the previous simulations, so to facilitate the sliding of the blocks.

Numerical experiments have shown that for $\mu \geq 0.15$ the blocks do not exhibit appreciable movements. Sliding and collapse become evident when $\mu = 0.1$, and this is the case to which Figures 14 refer to. In the simulations the dead load is instantaneously applied at the time $t = 0$, which is a very drastic assumption that does not consider that the dome is very slowly loaded during its construction. However, on the one hand, the detailed analysis of the static states at various construction phases goes beyond the scope of the present article; on the other hand, the simulations now presented, where the friction coefficient is unrealistically decreased until sliding occurs, are purely theoretical, and for sure a very low friction would be the most critical when the dome is not completely vaulted. Finally, recall that the kinematic theorem of limit analysis [22] indicates that the limit load multiplier does not depend upon the eigenstress states that are possibly present on the structure, such as those consequent to a gradual construction. Albeit tentatively, this conclusion may be applied also to the case at hand for which the theorems of limit analysis are not rigorously

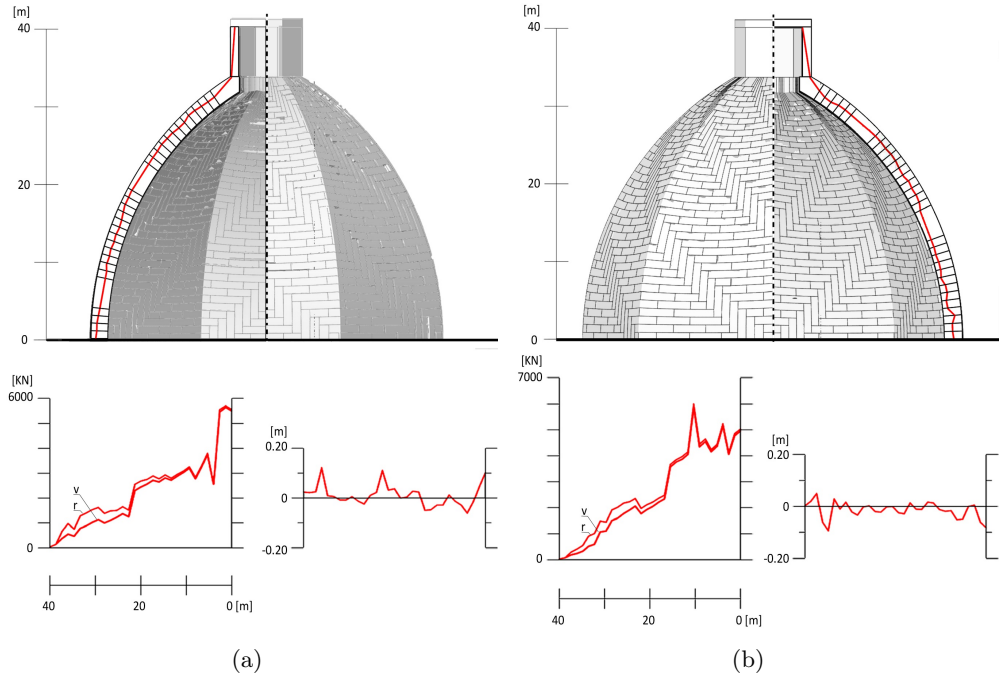

(a) (b)

Figure 13: Meridian thrust line in the Brunelleschi dome model, with quantitative indication of the contact wrenches. a) Middle of the sail. b) Corner rib.

applicable because, as indicated in Section 2.2 and discussed at length in [9], the solution relies upon an associative frictional model but only at the time-step level, whereas the dilatation effects are annihilated at the successive steps[5].

Figure 14(a) represents the situation at $t = 1$ s. What is evident is that the cracks open in the lower part of the dome, where the hoop stress is tensile, and they are particularly concentrated at the herringbone spirals. This is confirmed by Figure 14(b) corresponding to $t = 2$ s, which shows that sliding is very limited where the blocks are laid according to the long axis, whereas the vertical blocks represent a real wound in the structural texture. Collapse starts when sliding overcomes the width of the horizontal joints of the blocks forming the herringbone spirals: eventually, at $t = 2.5$ s, a vertical gap is present between the upper surface of the herringbone shown in Figure 14(c), and the overlying part of the dome, so that the latter part is no longer supported from below and falls down. The final stage of the collapse, represented in Figure 14(d) at $t = 3$ s, confirms the complete collapse of the herringbone spirals, accompanied by the rotation of the blocks and their falling apart.

The fact that the herringbones represent a very weak point with respect to the capacity of the dome to withstand tensile hoop stresses, is in agreement with the conclusions set forth in [9], where the tensile strength of the horizontal layers is taken into account. Usually, this

[5] As observed by Drucker [18], if normality fails the classical theorems of limit analysis are no longer valid for frictional sliding. Normality condition is preserved in the case of associative friction.

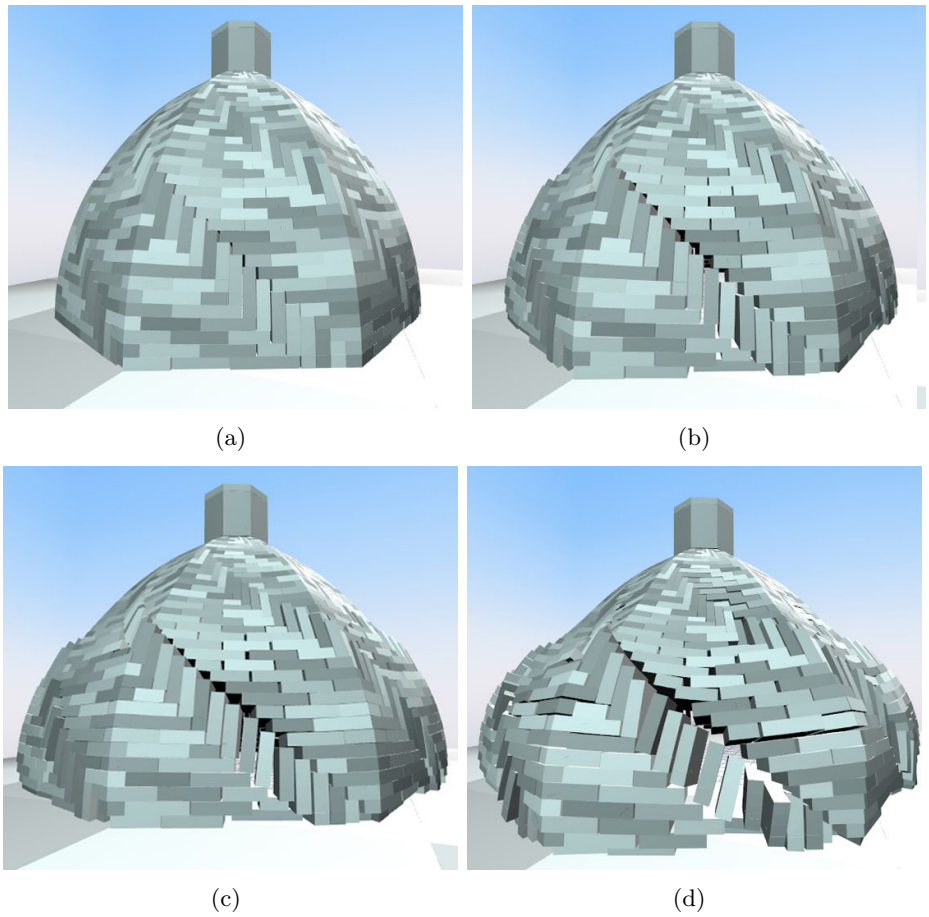

(a) (b)

(c) (d)

Figure 14: Collapse of the Brunelleschi model with friction coefficient $\mu = 0.1$ at different times t: a) $t = 1$ s, b) $t = 2$ s, c) $t = 2.5$ s, d) $t = 3$ s.

is done by assuming a moderate tensile strength of the bulk material, but this seems to result more in a facilitation of the numerical analysis than in an improvement of the accuracy of the response. In [9], the resistance to horizontal tensile forces is attributed to the mortar layers, and depends on the vertical pressure in the way specified by Coulomb friction law. With this assumption, the aspect ratio of the blocks that form the structure becomes of paramount importance for the determination of the collapse mechanism, because the thinner the blocks, the higher is the force per unit meridian-length that is needed to provoke sliding, and *vice versa*.

The numerical experiments recorded here, and in particular the discussion of Figure 11, indicate that the bricks forming the herringbone act as stress concentrators for the meridional contact forces. Likewise, as evident in Figure 9(b), this provokes that the contact forces diminish in those horizontal blocks adjacent to the vertical blocks, which consequently become prone to sliding. But the most important aspect to consider is that the possibility

of equilibrating the hoop stress depends upon the aspect ratio of the blocks: the highest strength capacity in the direction of the parallels is obtained when the blocks are large and thin. This fact has been fully confirmed by the numerical experiments reported in [9], and here it is once more evident, because the blocks laid vertically are more prone to sliding than the blocks laid horizontally. This is why the herringbone, where the bricks are laid vertically, represents a real wound in the dome surface, whose negative effect is only partially mitigated by the spiral pattern. Indeed, if the herringbone were vertical, following the direction of a meridian, the dome could be easily split by a moderate tensile stress demand along the parallels.

4 Conclusions

In masonry constructions the bond pattern of the constituent bricks is of paramount importance, because it determines structural stiffness and load beating capacity. This aspect can be considered with a Non-Smooth-Contact-Dynamics (NSCD) approach, that here has been implemented in a custom simulator interfaced with a parametric design software so to generate complex meshes and visualize contact forces. When dealing with complex geometries, the challenging problem is the high indeterminacy of the contact reactions, consequent from the hypothesis of rigidity of the constituent blocks. This difficulty is bypassed with the robust handling of a regularization procedure, which consists in the introduction of a numerical compliance at each contact point. Such a compliance can model the deformability of the mortar joints, but its precise evaluation is not crucial, because the location and size of the contact reactions does not sensibly depend upon the value of the compliance, at least in a certain significant range. The numerical solution poses further difficulties, because the bond pattern is in general characterized by non-convex blocks and degenerated (highly undetermined) contacts between coplanar facets, which require a careful implementation of contact detection algorithms.

Numerical experiments have been presented for the very challenging case represented by the *cupola* of Santa Maria del Fiore in Florence, characterized by a conical layering of the bricks that defines a dome of revolution *hidden* in the octagonal shape. The structural differences between the ingenious construction adopted by Brunelleschi, on the one hand, and pure domes of revolutions and octagonal groin vaults with horizontal corbelling, on the other hand, have been highlighted in simplified, though representative, model problems, solved with our NSCD custom software. In general, the Brunelleschi arrangement provides a regular flow of the meridian stresses and does not overload the ribs with respect to the middle of the sails, as in octagonal groin vaults. In any case, the herringbone spirals, inserted presumably for construction purposes, represent a heavy disturbance.

The model predicts that, with respect to the distribution of meridian stresses, the herringbone is more stressed than the neighboring parts because, taking into account that the deformability is concentrated at the contact points *via* the introduced regularizing compli-

ance, the herringbone is stiffer since a less number of horizontal joints is encountered when the meridian passes though it. On the other hand, the herringbone has very limited capacity of equilibrating the hoop stresses because, as already discussed in [9] from a more general point of view, the frictional shear forces acting at the horizontal joints are small. This is the consequence of the fact the brickwork at the herringbone is vertical narrow, whereas it is horizontal in the neighboring parts. Numerical experiments, in which the friction coefficient has been gradually reduced, demonstrate that collapse is indeed associated with the shear sliding of the bricks right at the herringbone spirals.

Far from being complete and exhaustive, nevertheless this study confirms, with reference to one of the most famous and well-known masterpieces of the Italian Renaissance, the importance of the bond pattern of the masonry in complex spatial arrangements, and that the NSCD approach represents a powerful tool to analyze its structural implications. Further studies for the Florentine monument, which will necessitate an additional custom development of the NSCD simulator, will consider Brunelleschi's technique of "building without centering", taking into account that during the construction the mortar of the last-laid ring is fresh and, consequently, the associated friction coefficient is much smaller than in the dry joints. In this condition, certainly the herringbone will play the decisive role in preventing the sliding of the bricks.

Acknowledgements. The authors are grateful to Professor Silvia Briccoli Bati (University of Florence) for inspiring discussion during the preparation of this work. VB acknowledges the support of Abdullah Gül University, Turkey, under project number FUA-2017-85. GRC acknowledges the support of the Italian Ministry of University under grant MIUR-PRIN voce COAN 5.50.16.01 code 2015JW9NJT and of the Italian Civil Protection Department, Presidency of the Council of Ministers, under project ReLUIS-DPC 2014-2018.

References

[1] Leon Battista Alberti. *Leonis Baptistae Alberti Florentini Viri clarissimi De re aedificatoria*. N. Laurentus, 1485.

[2] L. Ambrosio, N. Fusco, and D. Pallara. *Functions of bounded variation and free discontinuity problems*. Oxford university press, Oxford, 2000.

[3] Mihai Anitescu. Optimization-based simulation of nonsmooth rigid multibody dynamics. *Math. Program.*, 105(1):113–143, 2006.

[4] Mihai Anitescu and Gary D. Hart. A constraint-stabilized time-stepping approach for rigid multibody dynamics with joints, contact and friction. *International Journal for Numerical Methods in Engineering*, 60(14):2335–2371, 2004.

[5] Mihai Anitescu and Alessandro Tasora. An iterative approach for cone complementarity problems for nonsmooth dynamics. *Computational Optimization and Applications*, 47(2):207–235, 2010.

[6] Lando Bartoli. *Filippo Brunelleschi*. Nardini, 1977.

[7] V. Beatini, G. Royer-Carfagni, and A. Tasora. A regularized non-smooth contact dynamics approach for architectural masonry structures. *Computers and Structures*, 187:88–100, 2017.

[8] V. Beatini, G. Royer-Carfagni, and A. Tasora. Modelling the shear failure of segmental arches. *Submitted for publication*, 474(2209), 2018.

[9] V. Beatini, G. Royer-Carfagni, and A. Tasora. The role of frictional contact of constituent blocks on the stability of masonry domes. *Proceedings of the Royal Society A: Mathematical, Physical and Engineering Sciences*, 474(2209), 2018.

[10] Ernesto G. Birgin, Jos Mario Martnez, and Marcos Raydan. Nonmonotone spectral projected gradient methods on convex sets. *SIAM Journal on Optimization*, 10(4):1196–1211, 2000.

[11] C. Casapulla and A. Maione. Modelling the dry-contact interface of rigid blocks under torsion and combined loadings: Concavity vs. convexity formulation. *International Journal of Non-Linear Mechanics*, 99:86–96, 2018.

[12] C. Casapulla and F. Portioli. Experimental and analytical investigation on the frictional contact behavior of 3d masonry block assemblages. *Construction and Building Materials*, 78:126–143, 2015.

[13] B. Chetouane, F. Dubois, M. Vinches, and C. Bohatier. Nscd discrete element method for modelling masonry structures. *International Journal for Numerical Methods in Engineering*, 64(1):65–94, 2005.

[14] M. Coli, M. Haines, and P. Bianchini. Le pietre della cupola del brunelleschi. In *Quinto Congresso Nazionale Geologia e Turismo*, Bologna, June 4-5 2013. Available on line at: www.isprambiente.gov.it/public_files/geologia-e-turismo/28-COLI-HAINES-BIANCHINI-poster.pdf.

[15] Roberto Corazzi. The loxodromiccurve and the herringbone. *DisegnareCon*, 5(9):85–92, 2012.

[16] Erwin Coumans. http://bulletphysics.org, 2012.

[17] Salvatore Di Pasquale. *Brunelleschi. La costruzione della cupola di Santa Maria del Fiore*. Marsilio, 2002.

[18] Daniel Charles Drucker. Coulomb friction, plasticity and limit loads. *Journal of Applied Mechanics*, 21(1):71–74, 1954.

[19] F. Dubois and M. Jean. The non-smooth contact dynamic method: recent lmgc90 software developments and application. In Peter Wriggers and Udo Nackenhorst, editors, *Analysis and Simulation of Contact Problems*, pages 375–378. Springer Berlin Heidelberg, Berlin, Heidelberg, 2006.

[20] S.S. Keerthi E.G. Gilbert, D.W. Johnson. A fast procedure for computing the distance between complex objects in three-dimensional space. *Robotics and Automation*, 4(2):193–203, 1988.

[21] Andre Godard. *The Art of Iran*. Praeger, 1965.

[22] J. Heyman. Equilibrium of masonry arches. *Proceedings of the Institution of Civil Engineers. Engineering and Computational Mechanics*, 163:129–133, 2010.

[23] Toby Heyn, Mihai Anitescu, Alessandro Tasora, and Dan Negrut. Using krylov subspace and spectral methods for solving complementarity problems in many-body contact dynamics simulation. *International Journal for Numerical Methods in Engineering*, 95(7):541–561, 2013.

[24] M. Jean. The non-smooth contact dynamics method. *Computer Methods in Applied Mechanics and Engineering*, 177(3):235 – 257, 1999.

[25] Michel Jean. *Micromechanics of Granular Materials*, chapter Numerical Simulation of Granular Materials, pages 149–315. ISTE-Wiley, 2009.

[26] Ross King. *Brunelleschi's Dome. How a Renaissance Genius Reinvented Architecture*. Chatto & Windu, 2000.

[27] T. Koziara and N. Bićanić. A distributed memory parallel multibody contact dynamics code. *International Journal for Numerical Methods in Engineering*, 87(1-5):437–456, 2011.

[28] Giovanni Lancioni, Davide Gentilucci, Enrico Quagliarini, and Stefano Lenci. Seismic vulnerability of ancient stone arches by using a numerical model based on the non-smooth contact dynamics method. *Engineering Structures*, 119(Supplement C):110 – 121, 2016.

[29] Antonio Manetti. *Filippo Brunelleschi: sa vie, son oeuvre*. Ecole nationale superieure des Beaux-Arts, 1985.

[30] J.-J. Moreau. Unilateral contact and dry friction in finite freedom dynamics. In J. J. Moreau and P. D. Panagiotopoulos, editors, *Nonsmooth Mechanics and Applications*, pages 1–82. Springer Vienna, Vienna, 1988.

[31] J.-J. Moreau. Numerical aspects of the sweeping process. *Computer Methods in Applied Mechanics and Engineering*, 177(3-4):329 – 349, 1999.

[32] A. Pizzigoni. Brunelleschi's bricks. *Journal of the International Association for Shell and Spatial Structures*, 56(2):137–148, 2015.

[33] Xiuzhi Qu and Brent Stucker. A 3d surface offset method for stl-format models. *Rapid Prototyping Journal*, 9(3):133–141, 2003.

[34] Ali Rafiee, Marc Vinches, and Claude Bohatier. Application of the nscd method to analyse the dynamic behaviour of stone arched structures. *International Journal of Solids and Structures*, 45(25):6269 – 6283, 2008.

[35] Piero Sanpaolesi. *La Cupola di Santa Maria del Fiore. Il Progetto la Costruzione.* Edam, 1977.

[36] G. De Saxcé and Z.-Q. Feng. The bipotential method: A constructive approach to design the complete contact law with friction and improved numerical algorithms. *Mathematical and Computer Modelling*, 28(4):225 – 245, 1998.

[37] A. Tasora, M. Anitescu, S. Negrini, and D. Negrut. A compliant visco-plastic particle contact model based on differential variational inequalities. *International Journal of Non-Linear Mechanics*, 53(0):2 – 12, 2013. Multibody System Dynamics: A Selective Perspective.

[38] G.P.A.G. van Zijl. Modeling masonry shear-compression: Role of dilatancy highlighted. *Journal of Engineering Mechanics*, 130(11):1289–1296, 2004.